ACS Partner Journal

CHEM & BIO ENGINEERING

Open Access

This article is licensed under CC-BY-NC-ND 4.0

pubs.acs.org/ChemBioEng

Article

Sulfate-Pillared Adsorbent for Efficient Acetylene Separation from Carbon Dioxide and Ethylene

Published as part of Chem & Bio Engineering virtual special issue "Advanced Separation Materials and Processes".

Junhui Liu, Hua Shuai, Jingwen Chen, Shixia Chen, Zhenyu Zhou,* Jun Wang,* and Shuguang Deng*

Cite This: *Chem Bio Eng.* 2024, 1, 83−90

Read Online

ACCESS | Metrics & More | Article Recommendations | Supporting Information

ABSTRACT: The effective separation of acetylene (C_2H_2) from carbon dioxide (CO_2) and ethylene (C_2H_4) presents considerable challenges in the petrochemical industry. In this work, we report a novel sulfate-pillared (SO_4^{2-}) ultra-microporous material, denoted as SOFOUR-DPDS-Ni (SOFOUR = SO_4^{2-}, 4-DPDS = 4,4′-dipyridyldisulfide), for efficient C_2H_2 capture from both CO_2 and C_2H_4. The sulfate pillars play a crucial role in inducing robust negative electrostatic potentials within the intralayer cavities and interlayer channels, thereby facilitating the selective recognition of C_2H_2. As a result, SOFOUR-DPDS-Ni demonstrates a remarkable C_2H_2 adsorption capacity of 1.60 mmol g^{-1} at 0.01 bar, an exceptional selectivity of 174 for the 50/50 C_2H_2/CO_2 mixture, and a high selectivity of 65 for the 1/99 C_2H_2/C_2H_4 mixture. These impressive metrics position SOFOUR-DPDS-Ni as a promising adsorbent for benchmark C_2H_2 separations. Dynamic breakthrough experiments validate its outstanding performance in separating C_2H_2 from both the CO_2 and C_2H_4 mixtures. Computational simulations reveal the strong interactions between C_2H_2 and sulfate pillars, shedding light on the underlying mechanisms driving the adsorption process.

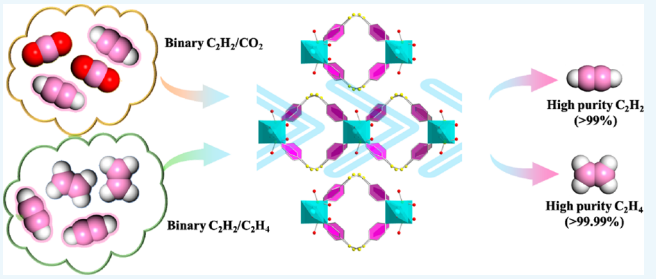

KEYWORDS: *sulfate-pillared, C_2H_2/CO_2 and C_2H_2/C_2H_4 separation, negative electrostatic potentials, breakthrough experiment*

1. INTRODUCTION

Acetylene (C_2H_2), a crucial industrial gas, plays a vital role in applications such as lighting, welding, and metal cutting, and serves as a feedstock for the production of various organic chemicals and polymers.[1] C_2H_2 is primarily produced through the steam cracking of hydrocarbons or partial combustion of methane, often coexisting with carbon dioxide (CO_2) in the crude product.[2] To further enhance its industrial utility, the separation of high-purity C_2H_2 (>99%) from C_2H_2/CO_2 mixtures is a fundamental requirement. However, due to the identical kinetic diameter (3.3 Å) and similar physicochemical properties (e.g., boiling points: C_2H_2, 189.3 K; CO_2, 194.7 K) (Table S1),[3] the separation of C_2H_2/CO_2 is recognized as one of the most challenging and demanding processes, typically involving significant energy consumption in traditional cryogenic distillation or solvent extraction.[4] Conversely, ethylene (C_2H_4), widely used as a feedstock in the chemical industry,[5] is typically produced through steam cracking and unavoidably contains trace impurities such as C_2H_2 (∼1%).[6] These trace C_2H_2 impurities can deactivate the catalyst during the ethylene polymerization process, necessitating their removal to low thresholds (< 40 ppm).[7] Currently, the removal of C_2H_2 relies on energy-intensive approaches, such as solvent absorption or partial hydrogenation. In this context, adsorptive separation based on porous adsorbents is considered as an energy-efficient alternative to separate C_2H_2 from CO_2 and C_2H_4 mixtures.[8,9]

Metal−organic frameworks (MOFs) as an emerging class of porous materials have recently shown exceptional performances in efficient C_2H_2 separations.[10−12] Compared to traditional adsorbents like zeolites and activated carbons, MOFs offer inherent modularity, enabling precise tuning of pore size/shape and pore chemistry through advanced pore engineering strategies.[13] This makes them well-suited for the efficient separation of challenging systems, such as C_2H_2/CO_2 and C_2H_2/C_2H_4 mixtures.[14−16] By exerting elaborate control over pore environments, MOFs with engineered anion-pillars in their frameworks can achieve preferential C_2H_2 adsorption based on specific host-guest interactions, indicating robust hydrogen-bonding or electrostatic interactions (Figure S1). Notably, ultra-microporous MOFs with fluorinated anion

Received: November 20, 2023
Revised: January 19, 2024
Accepted: January 21, 2024
Published: January 26, 2024

ACS Publications

© 2024 The Authors. Co-published by Zhejiang University and American Chemical Society

https://doi.org/10.1021/cbe.3c00094
Chem Bio Eng. 2024, 1, 83−90

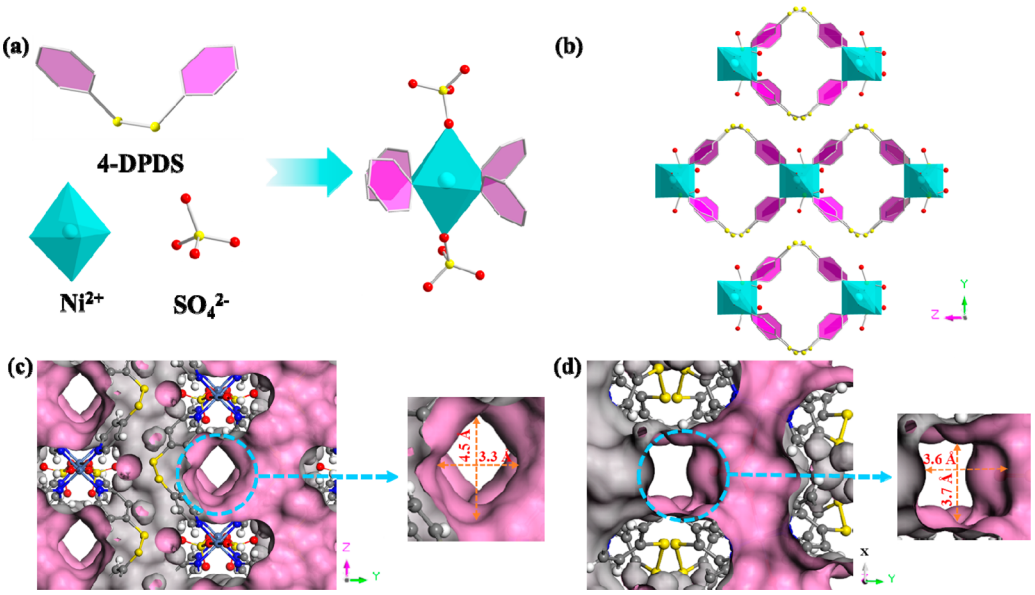

Figure 1. Illustration of the building blocks and local coordination environments of metal atoms and ligands (a). Intralayer cavities and interlayer channels of SOFOUR-DPDS-Ni (b). Window size of intralayer cavities (c). Window size of interlayer channels (d).

pillars (e.g., SiF_6^{2-}, TiF_6^{2-}, SnF_6^{2-}, $NbOF_5^{2-}$, and AlF_5^{2-})[17,18] exhibit excellent C_2H_2 adsorption at low pressures with high selectivity for C_2H_2/CO_2 and C_2H_2/C_2H_4 separation due to the strong interactions originating from high-density fluorine sites.[19−21] Moreover, another group of anion pillars containing high-density oxygen sites, such as $Cr_2O_7^{2-}$, CrO_4^{2-}, MoO_4^{2-}, and WO_4^{2-}, are integrated into MOFs to endow strong electronegativity for excellent C_2H_2 capture performance.[22,23] However, despite successful examples such as MFSIX, DICRO, and MOFOUR networks for C_2H_2 separation, they are typically limited to either C_2H_2/CO_2 or C_2H_2/C_2H_4 mixtures, except for a few recent examples like UTSA-300a,[24] ZU-12-Ni,[25] and $Co(4\text{-DPDS})_2CrO_4$.[23] Therefore, developing adsorbents capable of simultaneously separating both systems would be a desirable advancement that is worthy of further exploration.

Sulfate anions (SO_4^{2-}) possess abundant lone pair electrons in the oxygen atoms, enabling coordination with metal ions and potentially leading to the formation of ultra-microporous frameworks with the assistance of organic ligands.[26] Consequently, SO_4^{2-} has recently been employed as a novel anion pillar, driving the development of sulfate-based MOFs. In 2021, Zaworotko *et al.* reported the first sulfate-pillared hybrid ultra-microporous material (SOFOUR-1-Zn),[10] while our group has made further advancements by introducing a smaller ligand (TEPE = 1,1,2,2-tetra(pyridin-4-yl) ethene); the sulfate-pillared adsorbent (SOFOUR-TEPE-Zn) demonstrated exceptional molecule recognition ability for C_2H_2.[27] Inspired by pioneering C_2H_2 adsorbents based on fluorinated/oxygenated anion pillars, sulfate-pillared MOFs hold great potential in the field of C_2H_2 separation. In contrast to MOFs featuring pore "gate opening" due to the unrestricted rotation of linear pillars (*e.g.*, SiF_6^{2-}, TiF_6^{2-}, GeF_6^{2-}),[24,28,29] SO_4^{2-} as shorter tetrahedral anion pillars within frameworks only allow limited rotation, providing a high degree of pore confinement and multiple specific interaction sites to enhance selective C_2H_2 capture (Figure S2).[30]

Herein, we report a novel SO_4^{2-}-pillared adsorbent, SOFOUR-DPDS-Ni (4-DPDS = 4,4′-dipyridyl disulfide), where the tetrahedral SO_4^{2-} pillars enhance framework rigidity and prevent interlayer sliding (Figure 1a). Note that SOFOUR-DPDS-Ni features ideal intralayer cavity channels (3.3 × 4.5 Å^2) and interlayer pore channels (3.6 × 3.7 Å^2), closely matching the size of C_2H_2 molecules (3.32 × 3.34 × 5.70 Å^3). Furthermore, the abundant oxygen atoms in SO_4^{2-} and sulfur atoms in DPDS collectively create a strong negative electrostatic potential field for selective C_2H_2 recognition and binding. Thanks to these aspects, SOFOUR-DPDS-Ni not only displays a high adsorption capacity of C_2H_2 at low pressure (1.60 mmol g^{-1} at 0.01 bar) but also provides simultaneously benchmark C_2H_2/CO_2 (174) and C_2H_2/C_2H_4 (65) selectivity. The calculated appropriate C_2H_2 adsorption heat (Q_{st}) of 41.7 kJ mol^{-1} suggests the facile recovery of adsorbed C_2H_2 and adsorbent regeneration. Dynamic breakthrough experiments confirm its effective C_2H_2 capture performance for binary C_2H_2/CO_2 and C_2H_2/C_2H_4 gas-mixtures with good cyclability. Modelling studies reveal the strong host−C_2H_2 interactions, credited to the matched pore channels and strong electronegativity in frameworks.

2. EXPERIMENTAL SECTION

2.1. Materials. All of the reagents and solvents were obtained from commercial sources and used without further purification. Nickel sulfate hexahydrate ($NiSO_4{\cdot}6H_2O$, 99%, Aladdin), 4,4′-dipyridyl disulfide ($C_{10}H_8N_2S_2$, 98%, Xiya reagent), and methanol (CH_4O, anhydrous, 99.9%, Aladdin) were used as received without further purification. C_2H_2 (99.99%), CO_2 (99.99%), C_2H_4 (99.99%), N_2 (99.999%), He (99.999%), and mixed gas-mixtures of C_2H_2/CO_2 (50/50, *v*/*v*) and C_2H_2/C_2H_4 (50/50, *v*/*v* and 1/99, *v*/*v*) were purchased from Nanchang Guoteng Gas Co., Ltd (China).

2.2. Synthesis of SOFOUR-DPDS-Ni. $NiSO_4{\cdot}6H_2O$ (0.2 mmol, 0.0526 g) was added to a solution of 4-DPDS (0.4 mmol, 0.0881 g) in 20 mL of MeOH and stirred at room temperature for 24 h. SOFOUR-DPDS-Ni was obtained as a light blue powder and washed with 100 mL MeOH, followed by drying for 6 h at room temperature (yield: 1226 mg).

2.3. Gas Adsorption Measurements. Single-component isotherms of C_2H_2, CO_2, and C_2H_4 were measured up to 1 bar at 273, 298, and 323 K on a Micromeritics 3Flex adsorption apparatus (Micromeritics Instruments, USA). Kinetic adsorptions of C_2H_2,

https://doi.org/10.1021/cbe.3c00094
Chem Bio Eng. 2024, 1, 83−90

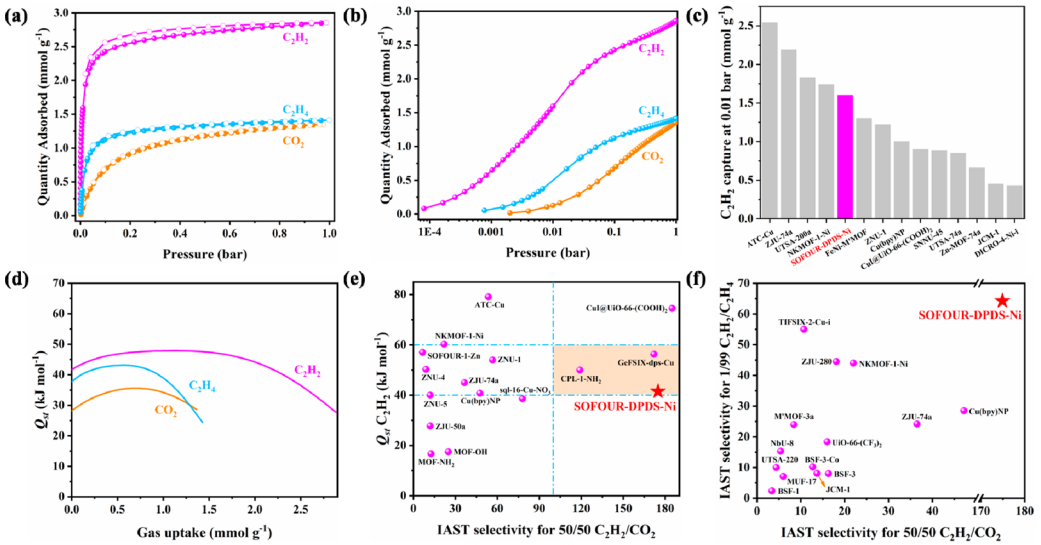

Figure 2. Pure-component adsorption isotherms of C_2H_2, CO_2, and C_2H_4 in SOFOUR-DPDS-Ni at 298 K (a). C_2H_2, CO_2, and C_2H_4 adsorption isotherms in the logarithmic form of SOFOUR-DPDS-Ni at 298 K (b). Comparison of C_2H_2 uptakes with those of other best-performing materials at 0.01 bar and 298 K (c). Isosteric heats of adsorption (Q_{st}) of C_2H_2, CO_2, and C_2H_4 were calculated from adsorption isotherms for SOFOUR-DPDS-Ni (d). Comparison of C_2H_2 Q_{st} and 50/50 C_2H_2/CO_2 selectivity with state-of-the-art adsorbents (e). Comparison of 50/50 C_2H_2/CO_2 and 1/99 C_2H_2/C_2H_4 selectivities with leading adsorbents (f).

CO_2, and C_2H_4 were obtained on an Intelligent Gravimetric Analyzer (IGA-100, HIDEN). Approximately 100 mg powder samples were evacuated under high vacuum (<5 μm of Hg) at 80 °C for 12 h before adsorption measurements, and the free space of the system was measured by using helium gas. Liquid nitrogen, liquid argon, and dry ice were used for adsorption isotherms at 77, 87, and 195 K, the pore size distribution was calculated based on CO_2 adsorption isotherms at 195 K.

2.4. Breakthrough Experiments. The breakthrough experiments were conducted in a stainless-steel column (4.6 mm inner diameter ×200 mm) manually packed with the weight of 0.7428 g of activated SOFOUR-DPDS-Ni. The column was initially purged with a helium flow (10 mL min^{-1}) at room temperature for 10 h before breakthrough tests. The binary mixture of C_2H_2/CO_2 (50:50, *v/v*) and C_2H_2/C_2H_4 (50:50, *v/v* and 1:99, *v/v*) was introduced at a flow rate of 2.0 and 5.0 mL min^{-1}, respectively. The outlet gas from the column was monitored using a mass spectrometer or gas chromatography for continuous sampling gas analysis. After the breakthrough tests, the columns packed with adsorbent samples were regenerated by purging helium gas of 10 mL min^{-1} at 60 °C for 12 h. The outlet composition during desorption was continuously monitored by a mass spectrometer or gas chromatography until a complete regeneration was achieved.

3. RESULTS AND DISCUSSION

3.1. Structure and Characterization. SOFOUR-DPDS-Ni was synthesized by simply reacting $NiSO_4·6H_2O$ with 4-DPDS in a methanol solution at room temperature. It is noteworthy that the reaction must be conducted under anhydrous conditiosn, as H_2O molecules exhibit a stronger coordination ability compared to SO_4^{2-} anions, potentially occupying the coordination site for Ni^{2+} ions.[31] Despite extensive efforts, we failed to obtain high-quality single crystals of SOFOUR-DPDS-Ni for single-crystal X-ray diffraction (SCXRD) analysis. Rietveld refinement of powder X-ray diffraction (PXRD) data indicated that the as-synthesized SOFOUR-DPDS-Ni crystallizes in the orthorhombic crystal system with cell parameters of a = 10.5377, b = 14.2957, c = 19.8289 (Figure S3, Tables S2 and S3).[32] The PXRD pattern of SOFOUR-DPDS-Ni exhibits excellent agreement with the simulated XRD profile, confirming the high purity of the prepared bulk sample (Figure S3). In Figure S4, Ni^{2+} ions adopt a six-coordinated distorted octahedral coordination environment. Specifically, each Ni^{2+} coordinates with four 4-DPDS ligands, forming double-chains of $[Ni(4\text{-}DPDS)_2]_n$ (Figure 1b). These chains are further pillared by two tetrahedral SO_4^{2-} anions occupying axial positions of Ni^{2+} ions, resulting in the formation of 2D $[SOFOUR\text{-}DPDS\text{-}Ni]_n$ layers exhibiting *sql* topology with intralayer channels of 3.3 × 4.5 Å^2 (Figure 1c). The adjacent 2D layers are then stacked and extended into the 3D structures through $\pi\cdots\pi$ interactions among pyridyl rings of 4-DPDS and p$\cdots\pi$ interactions between S atoms and pyridyl rings, resulting in narrow interlayer channels (3.6 × 3.7 Å^2) with negative electrostatic potentials (Figure 1d).

The PXRD patterns of SOFOUR-DPDS-Ni remain unchanged after activation, suggesting the rigidity of its framework (Figure S5). This rigidity is attributed to the formation of unparallel stacked frameworks with adjacent 2D layers pillared by tetrahedron SO_4^{2-} ions, effectively restricting the layer-to-layer sliding following guest molecule removal. This feature is advantageous compared to flexible frameworks linked by linear pillars (Figure S2).[33] Additionally, no gate-opening or stepwise adsorption behavior is observed in the adsorption isotherms of C_2H_2, CO_2, and C_2H_4 at different temperatures, validating the rigid structure pillared by tetrahedron SO_4^{2-} (Figure S6). All of this evidence demonstrates that SOFOUR-DPDS-Ni possesses a rigid skeleton suitable for C_2H_2 capture. The rigid frameworks with limited rotation should enable high degrees of pore confinement.

The structural integrity of SOFOUR-DPDS-Ni remains intact even after immersion in various organic solvents for 7 days, hot water at 60°C for 2 h, HCl (pH = 3 and 5), H_2O (pH = 7), and NaOH (pH = 9 and 11) solution for 1 day, and exposure to air for 13 months, indicating its exceptional stability (Figures S7 and S8). Furthermore, thermogravimetric analysis (TGA) revealed the removal of guest molecules at 383

https://doi.org/10.1021/cbe.3c00094
Chem Bio Eng. 2024, 1, 83−90

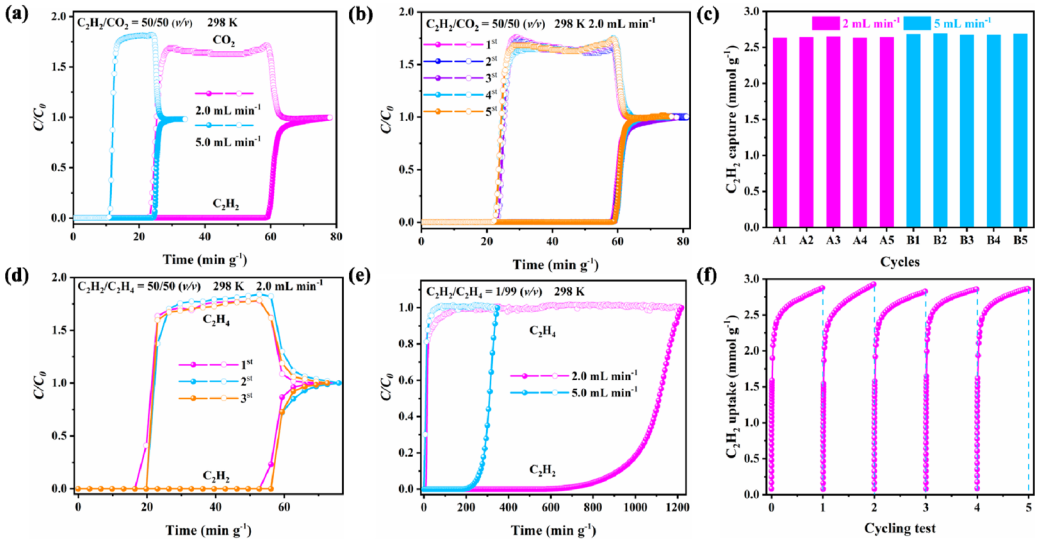

Figure 3. Experimental column breakthrough curves for the C_2H_2/CO_2 (50/50, *v*/*v*) binary mixture under the flow rate of 2.0 and 5.0 mL min^{-1} at 298 K and 1.0 bar (a). Cycling dynamic breakthrough tests were conducted for C_2H_2/CO_2 (50/50, *v*/*v*) under the flow rate of 2.0 mL min^{-1} on SOFOUR-DPDS-Ni (b). Cycling dynamic adsorption capacity of C_2H_2 for C_2H_2/CO_2 (50/50, *v*/*v*) by SOFOUR-DPDS-Ni under the flow rate of 2.0 and 5.0 mL min^{-1} (c). Cycling dynamic breakthrough tests were carried out for C_2H_2/C_2H_4 (50/50, *v*/*v*) under the flow rate of 2.0 mL min^{-1} on SOFOUR-DPDS-Ni (d). Experimental column breakthrough curves for the C_2H_2/C_2H_4 (1/99, *v*/*v*) binary mixture under the flow rate of 2.0 and 5.0 mL min^{-1} at 298 K and 1.0 bar (e). Continuous five C_2H_2 adsorption isotherms of SOFOUR-DPDS-Ni at 298 K (f).

K, while maintaining structural stability up to 473 K (Figure S9). Different temperature PXRD patterns revealed that SOFOUR-DPDS-Ni shows a high thermal stability up to 180 °C (Figure S10). The permanent porosity of the activated sample was examined by using CO_2 adsorption isotherms at 195 K (Figure S11). The type-I adsorption behavior reveals the inherent microporous character of SOFOUR-DPDS-Ni. The Brunauer−Emmett−Teller (BET) surface area is calculated to be 270 m^2 g^{-1} with a total pore volume of 0.15 cm^3 g^{-1}. The median pore size is determined to be 4.7 Å using the Horvath−Kawazoe model (Figure S12). Moreover, the porosity of SOFOUR-DPDS-Ni also validated the adsorption isotherms of 87 K Ar with the BET surface area of 94 m^2 g^{-1}. (Figure S13).

3.2. Adsorption and Separation Performances. Single-component gas adsorption isotherms of C_2H_2, CO_2, and C_2H_4 on SOFOUR-DPDS-Ni were collected at 273, 298, and 323 K, respectively (Figures 2a and S6). A notable C_2H_2 sorption capacity of 2.87 mmol g^{-1} was achieved at 1.0 bar and 298 K (Figure 2a), accompanied by a moderate uptake of CO_2 (1.36 mmol g^{-1}) and C_2H_4 (1.41 mmol g^{-1}). The substantial differences in adsorption capacities highlight the favorable affinity between the frameworks and C_2H_2 molecules. Moreover, the C_2H_2 adsorption isotherm exhibits a sharp increase at the low-pressure range, suggesting strong host-guest interactions between C_2H_2 molecules and SOFOUR-DPDS-Ni. This characteristic makes it highly desirable for the selective removal of trace C_2H_2 gas from C_2H_4. Impressively, SOFOUR-DPDS-Ni demonstrates an outstanding adsorption capacity for C_2H_2, reaching 1.60 mmol g^{-1} at 0.01 bar, comparable to benchmark MOFs such as NKMOF-1-Ni (1.74 mmol g^{-1}),[34] FeNi-M'MOF (1.3 mmol g^{-1}),[35] ZNU-1 (1.22 mmol g^{-1}),[1] and Cu(bpy)NP (1.0 mmol g^{-1})[6] (Figure 2b and c). In contrast, the uptakes of CO_2 and C_2H_4 at 0.01 bar are recorded to be 0.13 and 0.49 mmol g^{-1}, with uptake ratios as high as 12.3 (C_2H_2/CO_2) and 3.3 (C_2H_2/C_2H_4). The specific preference and strong affinity for C_2H_2 molecules are further validated by the isosteric heats (Q_{st}) using the Clausius−Clapeyron equation based on the Virial fitting of adsorption isotherms at three temperatures (Figure S17, Table S5). Notably, the Q_{st} of C_2H_2 on SOFOUR-DPDS-Ni at near zero coverage is estimated to be 41.7 kJ mol^{-1}, higher than that of CO_2 (28.2 kJ mol^{-1}) and C_2H_4 (37.7 kJ mol^{-1}), suggesting a stronger binding strength for C_2H_2. On the other hand, the Q_{st} of C_2H_2 at 41.7 kJ mol^{-1} ranks in a moderate range (40−60 kJ mol^{-1}), allowing for both firm binding capability and energy-efficient regeneration (Figures 3e and S18). Kinetic adsorptions of C_2H_2, CO_2, and C_2H_4 were obtained on Intelligent Gravimetric Analyzer (IGA-100) (Figures S19 and S20), which basically reached adsorption saturation within four min, indicating the negligible kinetic separation effect on SOFOUR-DPDS-Ni.

To assess the separation performance of SOFOUR-DPDS-Ni for C_2H_2/CO_2 and C_2H_2/C_2H_4 mixtures, the ideal adsorbed solution theory (IAST) selectivity was calculated based on the fitted adsorption data using the dual-site Langmuir−Freundlich isotherm model (Figures S14−S16). SOFOUR-DPDS-Ni exhibits a high C_2H_2/CO_2 (50/50, *v*/*v*) selectivity of 40 at 0.01 bar and 298 K, gradually increasing to 174 at 1 bar (Figure S21). This value surpasses that of most reported materials including ZJNU-109 (3.8),[36] ZJNU-118 (4.46),[37] CPL-1-NH$_2$ (119),[2] GeFSIX-dps-Cu (172),[28] and ZNU-1 (56.6),[1] despite being lower than that of SIFSIX-dps-Cu (1787),[28] HOF-FJU-1 (6675),[38] Cu^I@UiO-66-(COOH)$_2$ (185),[39] and UTSA-300a (743)[24] (Figure 2e and Table S6). Importantly, there are few reports on adsorbents with moderate C_2H_2 Q_{st} and C_2H_2/CO_2 (50/50, *v*/*v*) separation selectivities exceeding 100 (Figure 2e). Furthermore, the IAST selectivity for C_2H_2/C_2H_4 (1/99, *v*/*v*) reaches as high as1413 at 0.01 bar but gradually decreases to 65 at 1.0 bar (Figure S21), surpassing many top-ranking adsorbents, including Cu(bpy)NP (28.5),[6] TIFSIX-2-Cu-i (55),[40] and NKMOF-1-Ni (44)[34] (Figure 2f). Notably, SOFOUR-DPDS-Ni sets a new benchmark for efficient separation of both C_2H_2/CO_2 and C_2H_2/C_2H_4 gas-mixtures with high selectivity (Figure 2f).

https://doi.org/10.1021/cbe.3c00094
Chem Bio Eng. 2024, 1, 83−90

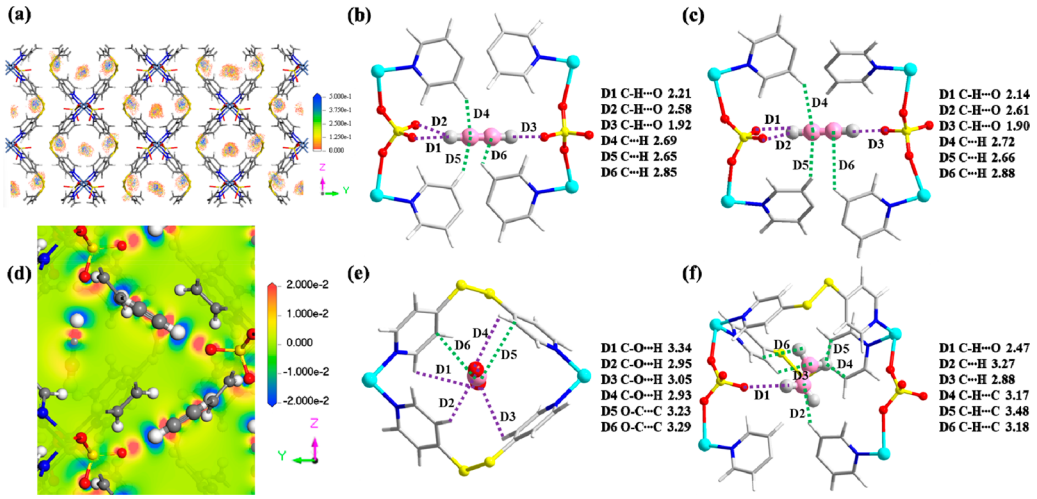

Figure 4. Computational simulations for the density distribution of C_2H_2 on SOFOUR-DPDS-Ni at 1 bar (a). DFT calculated binding site I of C_2H_2 in SOFOUR-DPDS-Ni (b). Binding site II of C_2H_2 (c). Charge density difference plots of the C_2H_2-loaded structure (d). Binding site I of CO_2 (e). Binding site of C_2H_4 (f).

3.3. Transient Breakthrough Experiment. Given the high separation potential, we evaluated the efficiency of SOFOUR-DPDS-Ni in separating challenging C_2H_2/CO_2 and C_2H_2/C_2H_4 mixtures using adsorption columns. Dynamic breakthrough experiments were conducted at room temperature, introducing binary mixtures of C_2H_2/CO_2 (50:50, *v/v*) and C_2H_2/C_2H_4 (50:50, *v/v* and 1:99, *v/v*) through a packed column filled with activated SOFOUR-DPDS-Ni at flow rates of 2.0 and 5.0 mL min^{-1}, respectively (Figure S22). Efficient C_2H_2/CO_2 separation is achieved by SOFOUR-DPDS-Ni at a flow rate of 2 mL min^{-1} (Figure 3a). CO_2 is eluted first at the column outlet around 23 min g^{-1}, while there is no detection of C_2H_2 until 59 min g^{-1}. The breakthrough interval between C_2H_2 and CO_2 is approximately 36 and 14 min g^{-1} at flow rates of 2 and 5 mL min^{-1}, respectively. Notably, the dynamic separation factor (α_{AC}) at two flow rates of equimolar C_2H_2/CO_2 mixture is determined to be 16 based on the breakthrough curves, outperforming benchmark adsorbents such as ZNU-5 (9.1),[41] ZNU-4 (5.4),[12] ZJU-50a (4.2),[42] and Cu(bpy)NP (3.9)[6] (Figure S23). To address industrial recyclability demands, multicycle breakthrough experiments were conducted under identical conditions (Figures 3b and S24). Markedly, no significant deterioration is observed in the breakthrough time and C_2H_2 capture capacity over five consecutive cycles (Figures 3b,c and S25), demonstrating its exceptional cyclability for C_2H_2/CO_2 separation and practical feasibility. Furthermore, the corresponding working capacity of C_2H_2 is calculated to be 2.64 and 2.67 mmol g^{-1} at flow rates of 2 and 5 mL min^{-1}, respectively. This aligns well with the equilibrium adsorption of C_2H_2 (2.87 mmol g^{-1}) under similar conditions (298 K and 1 bar) (Figures 3c and S24). Additionally, due to the weak binding affinity between CO_2 and SOFOUR-DPDS-Ni, most adsorbed CO_2 could be purged within a mere duration of 10 min under helium flow (10 mL min^{-1}) at 333 K (Figure S26). Consequently, high purity C_2H_2 (> 99%) can be obtained from 10 to 90 min during desorption process with an estimated productivity of 1.34 mmol g^{-1}.

In addition to demonstrating excellent performance in dynamic C_2H_2/CO_2 separation, SOFOUR-DPDS-Ni also exhibits desirable capabilities for C_2H_2/C_2H_4 separation. For the C_2H_2/C_2H_4 (50/50, *v/v*) gas-mixture, breakthrough of C_2H_4 occurs at 19.8 min g^{-1}, while C_2H_2 is eluted until 56.1 min g^{-1}, thus confirming its exceptional practicality in the separation of C_2H_2/C_2H_4 (Figure 3d). Furthermore, the good recyclability of SOFOUR-DPDS-Ni is also evident in this context, (Figure 3d). Meanwhile, for the C_2H_2/C_2H_4 (1/99, *v/v*) mixture, the C_2H_4 is detected at 18.0 min g^{-1}, and notably, C_2H_2 could be retained in the column for an impressive period up to 582 min g^{-1} at the flow rate of 2 mL min^{-1} (Figure 3e). During this process, C_2H_4 with impressive purity of 99.99% is obtained and the corresponding productivity reaches as high as 58.9 mmol g^{-1} on SOFOUR-DPDS-Ni (Figures 3e and S27). The proposed adsorbent also delivers remarkable performance in achieving efficient separation of C_2H_2/C_2H_4 (1/99, *v/v*) at the flow rate of 5 mL min^{-1} (Figure 3e). Cycled breakthrough experiments of SOFOUR-DPDS-Ni for C_2H_2/C_2H_4 (1/99, *v/v*) were conducted and the five breakthrough curves exhibits a high degree of coincidence, confirming its excellent recyclability and regeneration capability for C_2H_2 separation (Figures S28 and S29). Considering the potential influence and competitive adsorption of moisture in practical processes, we carried out breakthrough experiments of a C_2H_2/CO_2 (50/50, *v/v*) and C_2H_2/C_2H_4 (50/50, *v/v*) mixture under humid conditions (relative humidity = 53.8%). The similar breakthrough curves of C_2H_2/CO_2 and C_2H_2/C_2H_4 are observed under dry and humid conditions, suggesting the good water vapor resistance of SOFOUR-DPDS-Ni (Figures 3, S30, and S31). Additionally, five successive C_2H_2 adsorption curves show intact C_2H_2 uptakes, and no significant decrease in the uptake capacity of C_2H_2 after soaking in CH_3OH or CH_3CN for 3 days, hot water at 60 °C for 2 h and breakthrough experiments, demonstrating the multiple availability and good stability of SOFOUR-DPDS-Ni for C_2H_2 adsorption (Figures 3f and S32).

3.4. Modeling Simulation Studies. To gain a comprehensive understanding of the adsorption behavior of C_2H_2, CO_2, and C_2H_4 in SOFOUR-DPDS-Ni, theoretical molecular simulations using the grand canonical Monte Carlo (GCMC) and electrostatic potential distribution (EPD) for SOFOUR-DPDS-Ni were conducted. The distribution density of C_2H_2 was explored at 0.01 and 1 bar of (Figures S33 and S34). Evidently, C_2H_2 molecules are distributed in both interlayer

https://doi.org/10.1021/cbe.3c00094
Chem Bio Eng. 2024, 1, 83−90

channels and intralayer cavities, with preferential adsorptions in interlayer channel (Figure 4a). In contrast, the CO_2 and C_2H_4 molecules primarily reside in intralayer cavities until the pressure increases to 1 bar. Generally, the distribution density of C_2H_2 on the SOFOUR-DPDS-Ni skeleton exceeds that of CO_2 and C_2H_4 at 0.01 and 1.0 bar, respectively, aligning with the experimental adsorption capacities. Furthermore, the adsorption phenomenon was further confirmed by the energy distribution curves of different gases (Figure S35). Consistent with the previously obtained Q_{st} values, the energy distribution values follow a similar order (C_2H_2 (11.513 kal mol^{-1}) > C_2H_4 (10.198 kal mol^{-1}) > CO_2 (9.261 kal mol^{-1})), indicating the preferential adsorption of C_2H_2 on SOFOUR-DPDS-Ni.

To further elucidate the high C_2H_2 adsorption capacity under low pressure, the EPD on SOFOUR-DPDS-Ni was calculated as (Figure S36). Remarkably, abundant negative electrostatic potential, primarily originating from the SO_4^{2-} pillars distributed in pores, is observed. The negative electrostatic potential of the frameworks, in principle, aligns well with the positive molecular electrostatic potential of C_2H_2, inducing specific recognition and intense binding with C_2H_2. Considering this, charge transfer analysis on gas-loaded structures was performed using first-principles dispersion-corrected density functional theory (DFT-D) calculations, where blue and yellow surfaces indicate charge accumulation and depletion, respectively (Figures 4d and S37). Strong potential-field-induced electron bias is observed between H atoms of C_2H_2 and O atoms of SO_4^{2-} pillars (Figures 4d and S37a). Specifically, the originally positively charged H atoms of C_2H_2 are surrounded by negative electrons, while abundant positrons situate around the O atoms of SO_4^{2-} pillars. This observed guest-host charge transfer suggests that electron-potential-derived mechanisms contribute to the strong affinity of C_2H_2 in SOFOUR-DPDS-Ni.[6,27] Conversely, no noticeable charge transfer is observed between frameworks and CO_2, C_2H_4 molecules (Figure S37b,c). These observations underscore the specific effect of a negatively charged pore environment on the recognition and preferential adsorption of C_2H_2.

Moreover, DFT-D calculations were carried out to illustrate the binding sites in SOFOUR-DPDS-Ni. Three optimized adsorption sites of C_2H_2 are revealed, with two strong adsorption sites (site I and site II) locating in interlayer channels and another one (site III) residing in intralayer cavities (Figures 4a–c and S38). In sites I and II, C_2H_2 molecules are captured by electronegative oxygen atoms of SO_4^{2-} anions from adjacent 2D $[SOFOUR\text{-}DPDS\text{-}Ni]_n$ layers via C–H···O bonds (1.90–2.61 Å) and hydrogen atoms on different pyridines via C···H bonds (2.65–2.88 Å) (Figure 4b,c). Such short distances indeed suggest a strong hydrogen bond among the C_2H_2, SO_4^{2-} pillars, and pyridyl rings. These strong interactions enable C_2H_2 to act as a connector, stabilizing the SOFOUR-DPDS-Ni framework.

Similarly, C_2H_2 in site III is also mainly trapped by oxygen atoms from SO_4^{2-} in the intralayer cavities via strong interactions of two C–H···O bonds (2.29–3.22 Å) and C···H bonds (2.72–2.97 Å) (Figure S38). The C_2H_2 molecule prefers to locate near the electronegative oxygen sites through strong electrostatic interactions, affirming successful trap design via the introduction of SO_4^{2-}. The short length of the tetrahedral SO_4^{2-} pillars affords a high degree of pore confinement, resulting in short bonding distances and intense host-guest interactions. The static binding energy of SOFOUR-DPDS-Ni for the three C_2H_2 adsorption sites is evaluated to be approximately 77.9, 79.4, and 60.5 kJ mol^{-1}, respectively.

In contrast, the two binding sites of CO_2 in interlayer channels and intralayer cavities exhibit much lower binding energy of 27.1 and 38.0 kJ mol^{-1}, respectively (Figures 4e and S39). The weak intermolecular interactions are mainly dominated by the O–C···O (2.93 Å), C–O···H (2.66–3.34 Å), and the O–C···C bonds (3.23–3.29 Å). Similarly, the interactions between C_2H_4 and SOFOUR-DPDS-Ni framework occur through C–H···O (2.47 Å), C···H (2.88 and 3.27 Å), and C–H···C (3.17–3.48 Å) bonds, with binding energy estimated to be 44.1 kJ mol^{-1} (Figure 4f). Consistent with the experimental observations, the affinity of SOFOUR-DPDS-Ni for C_2H_2 revealed by DFT-D is obviously higher than that of CO_2 and C_2H_4, thus explaining its superior C_2H_2 capture and separation.

4. CONCLUSIONS

In summary, we demonstrated the synthesis and characterization of a novel 2D tetrahedral sulfate-pillared ultramicroporous SOFOUR-DPDS-Ni, tailored for the efficient separation of C_2H_2 from challenging C_2H_2/CO_2 and C_2H_2/C_2H_4 gas mixtures. The strategic incorporation of tetrahedral SO_4^{2-} pillars imparted a distinctive combination of compact pore channels and a negative electrostatic environment of SOFOUR-DPDS-Ni. Consequently, SOFOUR-DPDS-Ni delivered an outstanding C_2H_2 capture capacity of 1.60 mmol g^{-1} at 0.01 bar, along with benchmark selectivities for both 50/50 C_2H_2/CO_2 (174) and 1/99 C_2H_2/C_2H_4 (65) mixtures. Dynamic breakthrough experiments validate the efficacy of C_2H_2 separation from CO_2 (50/50) and C_2H_4 (50/50 and 1/99) over multiple cycles, yielding high-purity products with exceptional productivity. Computational modeling elucidates the crucial role played by electronegative oxygen atoms and the well-defined channel environment facilitated by SO_4^{2-} pillars in separation performance.

■ ASSOCIATED CONTENT

Supporting Information

The Supporting Information is available free of charge at https://pubs.acs.org/doi/10.1021/cbe.3c00094.

Additional experimental details; PXRD patterns; TGA curve; structural stability tests; DFT calculation method; GCMC calculations; IAST selectivity calculations; separation factor calculations; Q_{st} calculations; diffusional time constant calculations; gas sorption measurements; and breakthrough experiments (PDF)

Accession Codes

Crystallographic data of SOFOUR-DPDS-Ni have been deposited in the Cambridge Crystallographic Date Centre (CCDC: 2260840).

■ AUTHOR INFORMATION

Corresponding Authors

Zhenyu Zhou − *Chemistry and Chemical Engineering School, Nanchang University, Nanchang, Jiangxi 330031, China*; Email: zhouzhenyu@ncu.edu.cn

Jun Wang − *Chemistry and Chemical Engineering School, Nanchang University, Nanchang, Jiangxi 330031, China*; orcid.org/0000-0001-5176-309X; Email: jwang7@ncu.edu.cn

https://doi.org/10.1021/cbe.3c00094
Chem Bio Eng. 2024, 1, 83–90

Shuguang Deng − *School for Engineering of Matter, Transport and Energy, Arizona State University, Tempe, Arizona 85287, United States;* orcid.org/0000-0003-2892-3504; Email: shuguang.deng@asu.edu

Authors

Junhui Liu − *Chemistry and Chemical Engineering School, Nanchang University, Nanchang, Jiangxi 330031, China*

Hua Shuai − *Chemistry and Chemical Engineering School, Nanchang University, Nanchang, Jiangxi 330031, China*

Jingwen Chen − *Chemistry and Chemical Engineering School, Nanchang University, Nanchang, Jiangxi 330031, China*

Shixia Chen − *Chemistry and Chemical Engineering School, Nanchang University, Nanchang, Jiangxi 330031, China*

Complete contact information is available at: https://pubs.acs.org/10.1021/cbe.3c00094

Notes

The authors declare no competing financial interest.

■ ACKNOWLEDGMENTS

The research work was supported by the National Natural Science Foundation of China (No. 22308142(Z.Z.), 22168023 and 22322807 (J.W.), and 22268029 (J.C.) and the Natural Science Foundation of Jiangxi Province (20232BAB213039,20232BCJ25075, and 20224ACB204003).

■ REFERENCES

(1) Wang, L.; Sun, W.; Zhang, Y.; Xu, N.; Krishna, R.; Hu, J.; Jiang, Y.; He, Y.; Xing, H. Interpenetration Symmetry Control within Ultramicroporous Robust Boron Cluster Hybrid MOFs for Benchmark Purification of Acetylene from Carbon Dioxide. *Angew. Chem. Int. Ed.* **2021**, *60* (42), 22865−22870.

(2) Yang, L.; Yan, L.; Wang, Y.; Liu, Z.; He, J.; Fu, Q.; Liu, D.; Gu, X.; Dai, P.; Li, L.; Zhao, X. Adsorption Site Selective Occupation Strategy within a Metal−Organic Framework for Highly Efficient Sieving Acetylene from Carbon Dioxide. *Angew. Chem. Int. Ed.* **2021**, *60* (9), 4570−4574.

(3) Sun, W.-Q.; Hu, J.-B.; Jiang, Y.-J.; Xu, N.; Wang, L.-Y.; Li, J.-H.; Hu, Y.-Q.; Duttwyler, S.; Zhang, Y.-B. Flexible Molecular Sieving of C_2H_2 from CO_2 by a New Cost-Effective Metal Organic Framework with Intrinsic Hydrogen Bonds. *Chem. Eng. J.* **2022**, *439*, No. 135745.

(4) Zhu, X.; Ke, T.; Zhou, J.; Song, Y.; Xu, Q.; Zhang, Z.; Bao, Z.; Yang, Y.; Ren, Q.; Yang, Q. Vertex Strategy in Layered 2D MOFs: Simultaneous Improvement of Thermodynamics and Kinetics for Record C_2H_2/CO_2 Separation Performance. *J. Am. Chem. Soc.* **2023**, *145* (16), 9254−9263.

(5) Wen, H.; Yu, C.; Liu, M.; Lin, C.; Zhao, B.; Wu, H.; Zhou, W.; Chen, B.; Hu, J. Construction of Negative Electrostatic Pore Environments in a Scalable, Stable and Low-Cost Metal-organic Framework for One-Step Ethylene Purification from Ternary Mixtures. *Angew. Chem. Int. Ed.* **2023**, *62* (44), No. e202309108.

(6) Liu, Y.; Liu, J.; Xiong, H.; Chen, J.; Chen, S.; Zeng, Z.; Deng, S.; Wang, J. Negative Electrostatic Potentials in a Hofmann-Type Metal-Organic Framework for Efficient Acetylene Separation. *Nat. Commun.* **2022**, *13* (1), 5515.

(7) Gu, X.-W.; Wu, E.; Wang, J.-X.; Wen, H.-M.; Chen, B.; Li, B.; Qian, G. Programmed Fluorine Binding Engineering in Anion-Pillared Metal-Organic Framework for Record Trace Acetylene Capture from Ethylene. *Sci. Adv.* **2023**, *9* (31), No. eadh0135.

(8) Laha, S.; Dwarkanath, N.; Sharma, A.; Rambabu, D.; Balasubramanian, S.; Maji, T. K. Tailoring a Robust Al-MOF for Trapping C_2H_6 and C_2H_2 Towards Efficient C_2H_4 Purification from Quaternary Mixtures. *Chem. Sci.* **2022**, *13* (24), 7172−7180.

(9) Yang, S.-Q.; Zhou, L.; He, Y.; Krishna, R.; Zhang, Q.; An, Y.-F.; Xing, B.; Zhang, Y.-H.; Hu, T.-L. Two-Dimensional Metal−Organic Framework with Ultrahigh Water Stability for Separation of Acetylene from Carbon Dioxide and Ethylene. *ACS Appl. Mater. Interfaces* **2022**, *14* (29), 33429−33437.

(10) Sensharma, D.; O'Hearn, D. J.; Koochaki, A.; Bezrukov, A. A.; Kumar, N.; Wilson, B. H.; Vandichel, M.; Zaworotko, M. J. The First Sulfate-Pillared Hybrid Ultramicroporous Material, SOFOUR-1-Zn, and Its Acetylene Capture Properties. *Angew. Chem. Int. Ed.* **2022**, *61* (8), No. e202116145.

(11) Li, H.; Liu, C.; Chen, C.; Di, Z.; Yuan, D.; Pang, J.; Wei, W.; Wu, M.; Hong, M. An Unprecedented Pillar-Cage Fluorinated Hybrid Porous Framework with Highly Efficient Acetylene Storage and Separation. *Angew. Chem. Int. Ed.* **2021**, *60* (14), 7547−7552.

(12) Xu, N.; Hu, J.; Wang, L.; Luo, D.; Sun, W.; Hu, Y.; Wang, D.; Cui, X.; Xing, H.; Zhang, Y. A TIFSIX Pillared MOF with Unprecedented Zsd Topology for Efficient Separation of Acetylene from Quaternary Mixtures. *Chem. Eng. J.* **2022**, *450*, No. 138034.

(13) Wang, X.; Yue, L.; Zhou, P.; Fan, L.; He, Y. Lanthanide−Organic Frameworks Featuring Three-Dimensional Inorganic Connectivity for Multipurpose Hydrocarbon Separation. *Inorg. Chem.* **2021**, *60* (22), 17249−17257.

(14) Pei, J.; Shao, K.; Wang, J.; Wen, H.; Yang, Y.; Cui, Y.; Krishna, R.; Li, B.; Qian, G. A Chemically Stable Hofmann-Type Metal−Organic Framework with Sandwich-Like Binding Sites for Benchmark Acetylene Capture. *Adv. Mater.* **2020**, *32* (24), No. 1908275.

(15) Sun, H.; Chen, F.; Chen, R.; Li, J.; Guo, L.; Liu, Y.; Shen, F.; Yang, Q.; Zhang, Z.; Ren, Q.; Bao, Z. Customizing Metal-Organic Frameworks by Lego-Brick Strategy for One-Step Purification of Ethylene from a Quaternary Gas Mixture. *Small* **2023**, *19* (21), No. 2208182.

(16) Zheng, F.; Chen, R.; Liu, Y.; Yang, Q.; Zhang, Z.; Yang, Y.; Ren, Q.; Bao, Z. Strengthening Intraframework Interaction within Flexible MOFs Demonstrates Simultaneous Sieving Acetylene from Ethylene and Carbon Dioxide. *Adv. Sci.* **2023**, *10* (9), No. 2207127.

(17) Wang, J.; Zhang, Y.; Zhang, P.; Hu, J.; Lin, R.-B.; Deng, Q.; Zeng, Z.; Xing, H.; Deng, S.; Chen, B. Optimizing Pore Space for Flexible-Robust Metal−Organic Framework to Boost Trace Acetylene Removal. *J. Am. Chem. Soc.* **2020**, *142* (21), 9744−9751.

(18) Zhang, Y.; Yang, L.; Wang, L.; Duttwyler, S.; Xing, H. A Microporous Metal-Organic Framework Supramolecularly Assembled from a Cu^{II} Dodecaborate Cluster Complex for Selective Gas Separation. *Angew. Chem. Int. Ed.* **2019**, *131* (24), 8229−8234.

(19) Cui, X.; Chen, K.; Xing, H.; Yang, Q.; Krishna, R.; Bao, Z.; Wu, H.; Zhou, W.; Dong, X.; Han, Y.; Li, B.; Ren, Q.; Zaworotko, M. J.; Chen, B. Pore Chemistry and Size Control in Hybrid Porous Materials for Acetylene Capture from Ethylene. *Science* **2016**, *353* (6295), 141−144.

(20) Zhang, Z.; Ding, Q.; Cui, J.; Cui, X.; Xing, H. Fine-Tuning Pore Dimension in Hybrid Ultramicroporous Materials Boosting Simultaneous Trapping of Trace Alkynes from Alkenes. *Small* **2020**, *16* (49), No. 2005360.

(21) Zhang, Z.; Cui, X.; Yang, L.; Cui, J.; Bao, Z.; Yang, Q.; Xing, H. Hexafluorogermanate (GeFSIX) Anion-Functionalized Hybrid Ultramicroporous Materials for Efficiently Trapping Acetylene from Ethylene. *Ind. Eng. Chem. Res.* **2018**, *57* (21), 7266−7274.

(22) Zheng, F.; Chen, R.; Ding, Z.; Liu, Y.; Zhang, Z.; Yang, Q.; Yang, Y.; Ren, Q.; Bao, Z. Interlayer Symmetry Control in Flexible-Robust Layered Metal−Organic Frameworks for Highly Efficient C_2H_2/CO_2 Separation. *J. Am. Chem. Soc.* **2023**, *145* (36), 19903−19911.

(23) Zheng, F.; Chen, R.; Liu, Y.; Yang, Q.; Zhang, Z.; Yang, Y.; Ren, Q.; Bao, Z. Strengthening Intraframework Interaction within Flexible MOFs Demonstrates Simultaneous Sieving Acetylene from Ethylene and Carbon Dioxide. *Adv. Sci.* **2023**, *10* (9), No. 2207127.

(24) Lin, R.-B.; Li, L.; Wu, H.; Arman, H.; Li, B.; Lin, R.-G.; Zhou, W.; Chen, B. Optimized Separation of Acetylene from Carbon Dioxide and Ethylene in a Microporous Material. *J. Am. Chem. Soc.* **2017**, *139* (23), 8022−8028.

(25) Jiang, M.; Cui, X.; Yang, L.; Yang, Q.; Zhang, Z.; Yang, Y.; Xing, H. A Thermostable Anion-Pillared Metal-Organic Framework

for C_2H_2/C_2H_4 and C_2H_2/CO_2 Separations. *Chem. Eng. J.* **2018**, *352*, 803−810.
(26) Luo, J.; Hong, M.; Wang, R.; Yuan, D.; Cao, R.; Han, L.; Xu, Y.; Lin, Z. Self-Assembly of Three Cd^{II}- and Cu^{II}-Containing Coordination Polymers from 4,4′-Dipyridyl Disulfide. *Eur. J. Inorg. Chem.* **2003**, *2003* (19), 3623−3632.
(27) Liu, X.; Zhang, P.; Xiong, H.; Zhang, Y.; Wu, K.; Liu, J.; Krishna, R.; Chen, J.; Chen, S.; Zeng, Z.; Deng, S.; Wang, J. Engineering Pore Environments of Sulfate-Pillared Metal-Organic Framework for Efficient C_2H_2/CO_2 Separation with Record Selectivity. *Adv. Mater.* **2023**, *35* (20), No. 2210415.
(28) Wang, J.; Zhang, Y.; Su, Y.; Liu, X.; Zhang, P.; Lin, R.; Chen, S.; Deng, Q.; Zeng, Z.; Deng, S.; Chen, B. Fine Pore Engineering in a Series of Isoreticular Metal-Organic Frameworks for Efficient C_2H_2/CO_2 Separation. *Nat. Commun.* **2022**, *13* (1), 200.
(29) Shen, J.; He, X.; Ke, T.; Krishna, R.; Van Baten, J. M.; Chen, R.; Bao, Z.; Xing, H.; Dincă, M.; Zhang, Z.; Yang, Q.; Ren, Q. Simultaneous Interlayer and Intralayer Space Control in Two-Dimensional Metal−Organic Frameworks for Acetylene/Ethylene Separation. *Nat. Commun.* **2020**, *11* (1), 6259.
(30) Zheng, F.; Guo, L.; Chen, R.; Chen, L.; Zhang, Z.; Yang, Q.; Yang, Y.; Su, B.; Ren, Q.; Bao, Z. Shell-like Xenon Nano-Traps within Angular Anion-Pillared Layered Porous Materials for Boosting Xe/Kr Separation. *Angew. Chem. Int. Ed.* **2022**, *61* (20), e202116686.
(31) Cordes, D. B.; Hanton, L. R.; Spicer, M. D. Six-Coordinated Cd(II) Centers as Four- or Six-Connected Nodes in Coordination Polymer Networks Containing Bis(4-Pyridyl)Amine. *Cryst. Growth. Des.* **2007**, *7* (2), 328−336.
(32) Zhang, P.; Zhong, Y.; Zhang, Y.; Zhu, Z.; Liu, Y.; Su, Y.; Chen, J.; Chen, S.; Zeng, Z.; Xing, H.; Deng, S.; Wang, J. Synergistic Binding Sites in a Hybrid Ultramicroporous Material for One-Step Ethylene Purification from Ternary C_2 Hydrocarbon Mixtures. *Sci. Adv.* **2022**, *8* (23), No. eabn9231.
(33) Zheng, F.; Chen, L.; Chen, R.; Zhang, Z.; Yang, Q.; Yang, Y.; Su, B.; Ren, Q.; Bao, Z. A Robust Two−Dimensional Layered Metal−Organic Framework for Efficient Separation of Methane from Nitrogen. *Sep. Purif. Technol.* **2022**, *281*, No. 119911.
(34) Peng, Y.-L.; Pham, T.; Li, P.; Wang, T.; Chen, Y.; Chen, K.-J.; Forrest, K. A.; Space, B.; Cheng, P.; Zaworotko, M. J.; Zhang, Z. Robust Ultramicroporous Metal-Organic Frameworks with Benchmark Affinity for Acetylene. *Angew. Chem. Int. Ed.* **2018**, *57* (34), 10971−10975.
(35) Gao, J.; Qian, X.; Lin, R.; Krishna, R.; Wu, H.; Zhou, W.; Chen, B. Mixed Metal−Organic Framework with Multiple Binding Sites for Efficient C_2H_2/CO_2 Separation. *Angew. Chem. Int. Ed.* **2020**, *59* (11), 4396−4400.
(36) Xu, T.; He, M.; Fan, L.; Zhou, P.; Jiang, Z.; He, Y. Engineering Ligand Conformation by Substituent Manipulation Towards Diverse Copper−Tricarboxylate Frameworks with Tuned Gas Adsorption Properties. *Dalton Trans.* **2021**, *50* (2), 638−646.
(37) Fan, L.; Yue, L.; Sun, W.; Wang, X.; Zhou, P.; Zhang, Y.; He, Y. Ligand Bent-Angle Engineering for Tuning Topological Structures and Acetylene Purification Performances of Copper-Diisophthalate Frameworks. *ACS Appl. Mater. Interfaces* **2021**, *13* (34), 40788−40797.
(38) Yang, Y.; Zhang, H.; Yuan, Z.; Wang, J.; Xiang, F.; Chen, L.; Wei, F.; Xiang, S.; Chen, B.; Zhang, Z. An Ultramicroporous Hydrogen-Bonded Organic Framework Exhibiting High C_2H_2/CO_2 Separation. *Angew. Chem. Int. Ed.* **2022**, *61* (43), No. e202207579.
(39) Zhang, L.; Jiang, K.; Yang, L.; Li, L.; Hu, E.; Yang, L.; Shao, K.; Xing, H.; Cui, Y.; Yang, Y.; Li, B.; Chen, B.; Qian, G. Benchmark C_2H_2/CO_2 Separation in an Ultra-Microporous Metal−Organic Framework via Copper(I)-Alkynyl Chemistry. *Angew. Chem. Int. Ed.* **2021**, *133* (29), 16131−16138.
(40) Chen, K.-J.; Scott, H. S.; Madden, D. G.; Pham, T.; Kumar, A.; Bajpai, A.; Lusi, M.; Forrest, K. A.; Space, B.; Perry, J. J.; Zaworotko, M. J. Benchmark C_2H_2/CO_2 and CO_2/C_2H_2 Separation by Two Closely Related Hybrid Ultramicroporous Materials. *Chem.* **2016**, *1* (5), 753−765.
(41) Wang, L.; Xu, N.; Hu, Y.; Sun, W.; Krishna, R.; Li, J.; Jiang, Y.; Duttwyler, S.; Zhang, Y. Efficient Capture of C_2H_2 from CO_2 and C_nH_4 by a Novel Fluorinated Anion Pillared MOF with Flexible Molecular Sieving Effect. *Nano Res.* **2023**, *16* (2), 3536−3541.
(42) Shao, K.; Wen, H.; Liang, C.; Xiao, X.; Gu, X.; Chen, B.; Qian, G.; Li, B. Engineering Supramolecular Binding Sites in a Chemically Stable Metal-Organic Framework for Simultaneous High C_2H_2 Storage and Separation. *Angew. Chem. Int. Ed.* **2022**, *61* (41), No. e202211523.

https://doi.org/10.1021/cbe.3c00094
Chem Bio Eng. 2024, 1, 83−90